Polymer 53 (2012) 5972–5981

Contents lists available at SciVerse ScienceDirect

Polymer

journal homepage: www.elsevier.com/locate/polymer

Hierarchically-responded assembly of block copolymer thin films with stimuli of varied solvent selectivity

Yu-Chi Lee [a], Ya-Sen Sun [a,*], Jiun-You Liou [a], Wei-Tsung Chuang [b,**]

[a] Department of Chemical and Materials Engineering, National Central University, Taoyuan 32001, Taiwan
[b] National Synchrotron Radiation Research Center, 101, Hsin-Ann Road, Hsinchu 30076, Taiwan

ARTICLE INFO

Article history:
Received 1 May 2012
Received in revised form
17 September 2012
Accepted 14 October 2012
Available online 22 October 2012

Keywords:
Copolymer thin films
Solvent annealing
Hierarchical self-assembly

ABSTRACT

Through a combination of micro-contact imprinting and block copolymer self assembly, a highly dewetting process of a symmetric diblock copolymer occurs, leading to hierarchical development of microstructures (microdroplets or microterraces) and nanodomains. The process is driven by the macroscopically hexagonal-ordered circular geometry of the PS-grafted pattern on silicon substrates and by solvent annealing in solvent vapors of varied selectivity. We investigate how relief P(S-*b*-4VP) microstructures adjust their internal nanostructures and microscopic shape on a patterned substrate in response to solvent vapors of varied selectivity. Whereas solvent annealing in THF vapor causes formation of nanosphere-comprised droplets with a hemispherical cap, solvent annealing in chloroform and acetone vapors leads to the development of terraced stacks of parallel-oriented lamellae. Each lamellar layer within the terraced stacks has the thickness of an entire PS-P4VP/P4VP-PS layer. In contrast, three types of relief microstructures, nanosphere-comprised terraces, nanocylinder-comprised droplets and nanolamella-comprised terraces, are found in a dynamic process under DMF vapor. For DMF-annealed terraces, the stacks comprise PS-P4VP lamellar layers and thus the thickness of each PS-P4VP lamellar layer is effectively quantized by a half thickness of one PS-P4VP/P4VP-PS layer. The variances in nanoscale and microscale structures are due to the adaption of stimuli-responsive polymer materials to surrounding environments under the confinement of the patterned substrate.

© 2012 Elsevier Ltd. All rights reserved.

1. Introduction

"Hierarchical self-assembly" is emerging as an elegant, bottom-up method for fabricating complex nanostructured and/or microstructured materials since it allows the concurrent switching of functional properties based on phase transitions of self-assembled structures in response to external stimuli [1–3]. Investigating the morphology, phase behavior and dynamics of hierarchical self-assembly in block copolymer (BCP) thin films still attracts great interest [4–13]. For BCP thin films, various complicated morphologies with ordering particularly at nanometer levels offer diverse and versatile benefits as potential nanotechnological applications [14–30]. However, microphase separation, by which nanodomains with periodical order are generated, only relies on weak- and short-range interactions so that short-range ordering emerges concurrently with the presence of a high density of defects [7]. To practice these applications, the key theme is to precisely and finely manipulate thin-filmed structures with long-range order through hierarchically directed assembly at different length levels by combinations of block copolymer self-assembly and other external driving forces. The most effective driving forces for correcting the loss of long-range lateral order in BCP thin films, for example, include graphoepitaxy [31,32], chemically patterned substrates [33], and solvent annealing [34].

Fabricating BCP thin films by spin coating combined with solvent annealing in solvent vapor turns out to be a simple, robust and an effective way to attain nanodomains with long-range lateral order and morphological diversity [34–36]. However, BCP thin films are inevitably prone to dewetting instabilities, which are generally mediated by the interplay between film thickness, polymer–surface as well as polymer–interface interactions and material viscosity [37–42]. For example, dewetting of BCP thin films spontaneously occurs to form relief micro-scale structures (such as holes or droplets) on a substrate when the thickness is incommensurate with an intrinsic spacing of ordered nanodomains [37–45]. After annealed at high temperature or exposed to solvents,

* Corresponding author. Tel.: +886 3422 7151x34205; fax: +886 3425 2296.
** Corresponding author.
E-mail addresses: yssun@cc.ncu.edu.tw (Y.-S. Sun), weitsung@nsrrc.org.tw (W.-T. Chuang).

0032-3861/$ – see front matter © 2012 Elsevier Ltd. All rights reserved.
http://dx.doi.org/10.1016/j.polymer.2012.10.031

the film stature becomes quantized in integer (symmetric wetting) or 1.5 integer (asymmetric wetting) units of the nanodomain spacing through film thickness undulation. Such dewetting instabilities, whereby a variety of relief microstructures can be generated, are a typical feature for symmetric BCP thin films [37–42].

Recently, Croll et al. investigated micro-scaled droplets of structured polystyrene-*block*-poly(methyl methacrylate) P(S-*b*-MMA) fluids on a flat substrate [8]. They observed that a symmetric P(S-*b*-MMA) droplet self-assembled into a stack of concentric circular disks with a terraced profile, and ascribed the terraced shape to the edge tension and edge repulsion. The terraced shape could further change to a hemisphere cap when the internal lamellar layers transformed into an isotropic disordered state [8]. Kim and coworkers studied the hierarchical self-assembly of polystyrene-*block*-poly(ethylene oxide), P(S-*b*-EO), on a chemical patterned substrate or with solvent-assisted wetting of the droplets on a flat substrate [4,5]. They found that the shape of dewetting-driven microstructures is hemispherical or terraced even though the internal nanostructures are all spherical nanodomains. Furthermore, Kim et al. found spontaneous lamellar alignment mediated by thickness-gradient in anisotropic microstructures [6,7]. Using surface-directed dewetting on the surface of patterned silsesquioxane micrometer-sized templates, Farrell et al. formed a variety of hierarchical structures from hexagonally-packed nanodot arrays within large-sized microdroplets to parallel nanocylinders with a shape of nano-ring circulating small-sized microdroplets [10]. These few examples illustrate that the development of microstructures in turn impose a confining space to influence the ordering, orientation and even morphology of internal nanodomains [4–7,10].

Here we present the hierarchical assembly behavior of stimuli-responsive polystyrene-*block*-poly(4-vinylpyridine), P(S-*b*-4VP), droplets to solvent vapors of varied selectivity on a patterned substrate. Patterned substrates were prepared by selectively grafting PS chains on SiO_x/Si by means of micro-contact imprinting. The PS-grafted regions have a hexagonal array on SiO_x/Si; therefore, solvent annealing caused dewetting-induced microdroplets with a microscopic order defined by the pattern of the PS-grafted substrates. Next we controlled variable surface fields with solvent vapors of varied solubility parameters, whereby internal building blocks within relief microstructures grew different microphase-separated nanodomains in response to the external environments. In addition, those relief microstructures adjusted their shape cooperatively with the spatial evolution of the nanostructured domains. With exposure to different solvent vapors, not only relief microstructures but also internal nanostructures can be reversely switchable.

2. Materials and experimental methods

2.1. Materials

Hydroxyl-terminated polystyrene (briefly denoted as PS_{4k}-OH: $M_n = 4$ kg/mol, index of polydispersity $I_p = 1.09$) and polystyrene-*block*-poly(4-vinylpyridine), P(S-*b*-4VP), ($M_n = 44$ kg/mol, $f_{ps} = 50\%$ and $f_{P4VP} = 50\%$, $I_p = 1.09$) were purchased (Polymer Source, Inc.) and used as received. Tetrahydrofuran (THF), chloroform, acetone, and N,N-dimethylformamide (DMF) were of analytical grade. The viscosities for the solvents at 25 °C are 0.456 (THF), 0.537 (chloroform), 0.306 (acetone) and 0.794 mPa s (DMF), respectively [46].

2.2. Surface modification of substrates by spin coating and by micro-contact imprinting

Bare silicon wafers were cleaned in a piranha solution (3:7 v/v 30% H_2O_2:H_2SO_4) for 40 min, rinsed with deionized water, and dried under flowing N_2. For substrates with surface modification grafted by PS brushes, PS–OH solutions (1 mass % in toluene) were spin-coated (1000 rpm, 1 min) on cleaned silicon wafers. The irreversibly grafted layers resulted from annealing (190 °C for 3 days) spin-coated films on hydroxylated silicon wafers under vacuum. Non-grafted materials were removed by sonication in toluene, followed by drying the substrates under flowing N_2. Patterned Si substrates can be prepared by selectively grafting PS chains onto the surface of SiO_x/Si using micro-contact imprinting (see Scheme 1). A sapphire master mold used for making poly(-dimethylsiloxane) (PDMS) stamps has circular holes arrayed with p6 mm hexagonal symmetry. The size of hexagon is 2 μm in diameter and the periodicity of the mold is 3 μm, respectively. Elastomeric PDMS stamps were fabricated by curing a mixture (10:1 by weight) of PDMS precursors (Sylgards 184, Dow Coring Corp) and curing agent on the pre-patterned sapphire. The mixture of PDMS precursors and curing agent was degassed first and then cured at 120 °C for 12 h under vacuum. To selectively grafting PS chains onto SiO_x/Si, an elastomeric PDMS stamp with a topographic micropattern was inked with a PS solution in toluene, and then was placed in conformal contact on SiO_x/Si substrates. After the period of 10 s micro-contact imprinting, the PDMS stamp was carefully peeled off and the substrate was dried by nitrogen. Thermal annealing at 190 °C was imposed on the inked substrates by which PS chains with hydroxyl chain-ends at the inked regions can covalently bond to the surface of SiO_x/Si. Each of the PS-grafted regions approximately has diameter 2 μm and thickness 4.1 nm and a separated distance 3 μm from its nearest neighbors.

2.3. Film preparation and annealing

The P(S-*b*-4VP) copolymer powders were dissolved in the mixture of toluene and tetrahydrofuran (THF) of the faction of

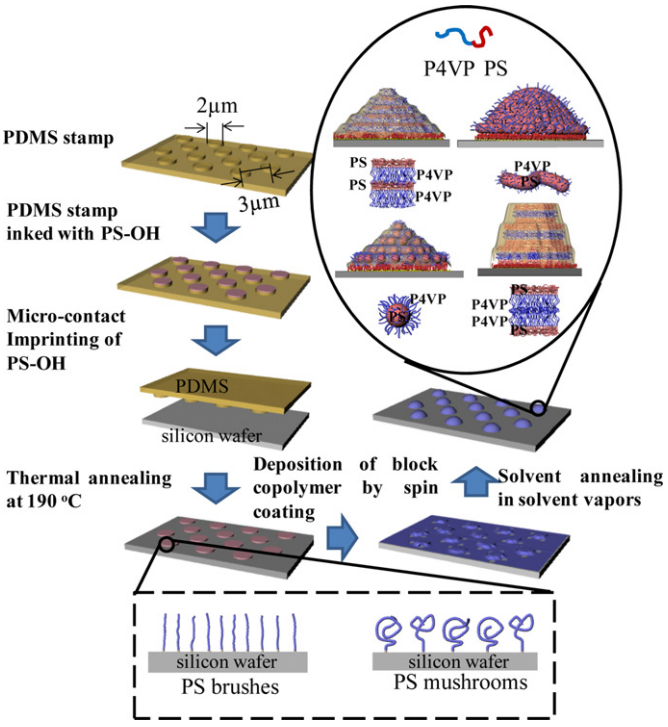

Scheme 1. Schematic illustrations of preparing patterned substrates having a hexagonal array of PS-grafted regions by micro-contact imprinting, and solvent-induced growing of hierarchical droplets or terraces in solvent vapors.

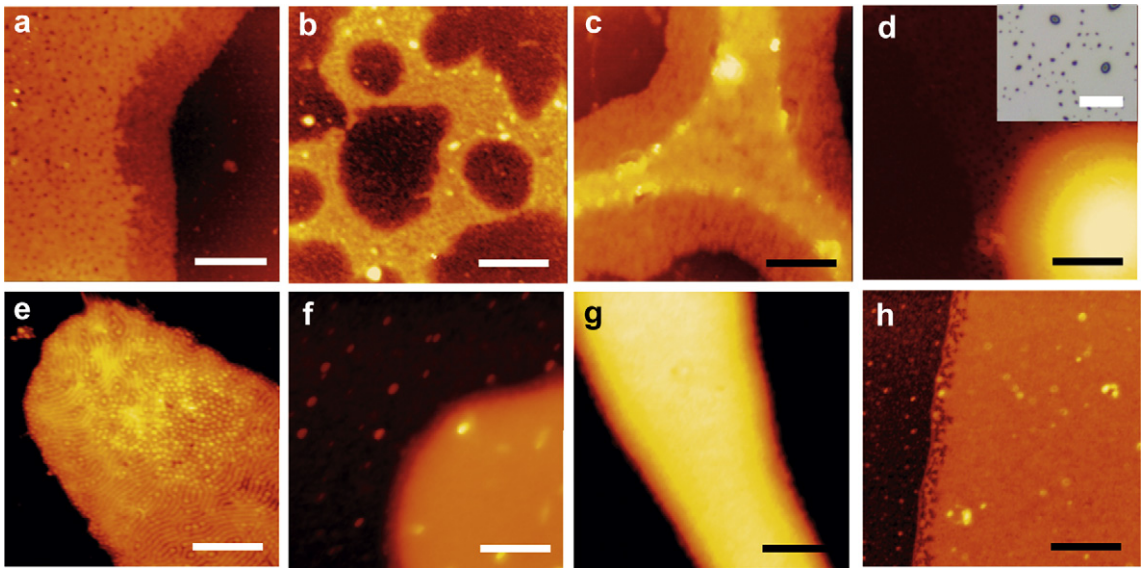

Fig. 1. AFM topographic images of the surface morphology of P(S-*b*-4VP) thin films on SiO_x/Si (a–d) and PS-SiO_x/Si (e–h) after exposure for 6 h to varied solvent vapors: (a, e) THF, (b, f) chloroform, (c, g) acetone and (d, h) DMF. (scale bar: 500 nm). The inset shown in image d represents OM image of dewetting-driven microscopic droplets of P(S-*b*-4VP) on SiO_x/Si in DMF vapor (scale bar: 10 μm).

70/30 at 70 °C for 2 h and cooled to room temperature (ca 25 °C) to yield 0.1 or 0.5 mass % polymer solutions. P(S-*b*-4VP) thin films of ca 29 nm were spread on substrates via spin coating (2000 rpm, 60 s). Then thin films were horizontally placed in a sealed jar of saturated solvent (THF, chloroform, acetone or DMF) vapors for different time periods of solvent annealing, at a maintained temperature 26 °C and relative humidity less than 10%.

2.4. Characterization

For studying the hierarchical self-assembly of thin films in response to vapors of varied selectivity, we observed the surface morphology by atomic force microscope (AFM, SPA400 Seiko) in the tapping mode and by optical microscope (OM, Olympus BX-BLA2) in the reflection mode. AFM images with scan ranges between 2 μm × 2 μm and 10 μm × 10 μm were recorded. We used aluminum-coated silicon cantilevers of length 150 μm, width 26 μm and thickness 3 μm; the force coefficient was approximately 7.4 N/m and the resonant frequency was 160 kHz. Measurements of grazing-incidence small-angle X-ray scattering (GISAXS) were performed with a Nano-Viewer (Rigaku) using CuK_α X-rays (40 kV and 30 mA) with wavelength $\lambda = 1.54$ Å at the Instrument Center of National Central University (NCU). Two-dimensional (2D) GISAXS patterns were collected with PLATUS 100 K of 83.8 × 33.5 mm^2 at incidence angle 0.2°, which is an optimal angle between the critical angles of samples and substrates. To obtain cross-sectional images of P(S-*b*-4VP) films under transmission electron microscopy (TEM), the thin films were embedded into epoxy and then cured at 60 °C after annealed in DMF vapor for 30 and 360 min and dried. Subsequently, the films were transferred onto the surface of epoxy from the PS-grafted substrates after dipped into liquid nitrogen. The embedded specimens were cut with the microtome. Thin sections (~100 nm thickness) of the embedded samples were microtomed on a Leica Reichert Ultracut-E-ultramicrotome; the sections were collected on copper grids and then stained with iodine vapor for ca 8 h, which preferentially stains the P4VP domains. TEM images were acquired on a JEOL TEM 2100 at 160 kV.

3. Results and discussion

3.1. Micellar morphologies on bare and PS-grafted substrates in solvent vapors of varied selectivity

In this study, free surface interactions were controlled with varied selectivity upon solvent annealing in solvents of four kinds – THF [solubility parameter δ: 18.6 $(MPa)^{0.5}$], chloroform [δ = 19 $(MPa)^{0.5}$], acetone [δ = 20.3 $(MPa)^{0.5}$] and DMF [δ = 24.8 $(MPa)^{0.5}$] [47]. The solvents were sorted as three categories by their solubility parameters: THF and chloroform are good solvents for PS [δ = 18.6 $(MPa)^{0.5}$] and DMF is a good solvent for P4VP [δ = 22.2 $(MPa)^{0.5}$]. Acetone is a neutral solvent, which is good for both the PS and P4VP block [47]. Two types of substrates were used – bare silicon substrates (SiO_x/Si) and substrates grafted with a layer of short PS chains (PS-SiO_x/Si) at a grafting density 0.65 chains/nm^2 – to control interactions at the substrate interface [48]. Bare substrates have a strong affinity to the P4VP block whereas grafting a layer of PS chains significantly suppresses the attractive interaction between SiO_x/Si and P4VP [48].

Before solvent annealing, the surface morphology on both SiO_x/Si and PS-SiO_x/Si reveals a collection of spherical-shaped micelles of monolayer thickness [47,48]. With exposing to the solvent vapors, the self-assembly and phase transitions of micelles reveal different behavior and pathways on SiO_x/Si or PS-SiO_x/Si (Fig. 1). For micelles on SiO_x/Si, annealing in vapors of THF, chloroform and acetone led to a wetting layer anchoring with the substrate surface whereas exposure to DMF vapor gave rise to dewetting-driven microscopic droplets (Fig. 1a–d). In contrast, for micelles on PS-SiO_x/Si, solvent annealing in the PS-preferable solvent vapors led to coexisting of spherical (majority) and cylindrical (minority) nanodomains (THF) or phase transitions to form lamellae (chloroform and acetone) (Fig. 1e–g). In THF vapor, the cylindrical nanodomains grew from the fusion of spherical micelles, and re-formed spherical micelles via micellar fission [47,48]. The height analysis demonstrates that the relief microstructures with exposure in chloroform and acetone vapors on PS-SiO_x/Si have thickness ca 30–40 nm (Fig. S1), which value is comparable to the thickness of a single full lamella that

comprises an entire PS-P4VP/P4VP-PS layer. With solvent annealing in DMF vapor, the micelles on PS-SiO_x/Si transited to form giant circular mats with PS chains being in contact with the grafted PS layer and with P4VP chains facing outward (Fig. 1h). A comparison for solvent-annealed micelles on SiO_x/Si and PS-SiO_x/Si demonstrates that the P(S-*b*-4VP) chains were preferentially in contact with the grafted PS and dewetted from the hydrophilic surface of SiO_x/Si under DMF vapor.

We further carried out grazing-incident small-angle X-ray scattering (GISAXS) to characterize the structural information of thin films on PS-SiO_x/Si without and with solvent annealing in the solvent vapors (see Fig. 2). Before solvent annealing, the surface of as-spun films was dominated by spherical micelles [47,48]. As Fig. 2a shows, the as-spun film reveals a set of diffraction truncation rods associated with the feature of the structure factor. That is, the truncation rods are related with the spatial order of nanodomains in the plane of PS-SiO_x/Si. For the as-spun micellar film, only the first-order diffraction rods are symmetrically present in the GISAXS pattern, indicating that the spherical nanodomains have a short-range order. Upon annealing in the solvent vapors, the diffraction rods diminished for the thin films with exposure in the vapors of DMF, chloroform or acetone (Fig. 2c–e) or depressed in intensity for the film with solvent annealed in THF vapor (Fig. 2b). As Fig. 1f–h shows, solvent annealing in chloroform, acetone and DMF led to the formation of parallel lamellae. Typically, the parallel lamellae should reveal scattering intensity maxima along the substrate normal (i.e., along the $q_\perp$ direction rather than along the $q_{//}$direction). However since there are only a few layers of parallel lamellae deposited on PS-SiO_x/Si, the intensity scattered by the lamellar structures is too weak to be discerned. By contrast, the thin film with exposure to THF vapor reveals diffraction rods with reduced intensity along the $q_{//}$direction. The GISAXS patterns demonstrate that upon solvent annealing, the surface morphologies of these thin films were dominated by either parallel lamellae or parallel cylinders with short-range lateral order.

In the following, we discuss the mechanism of formation of giant mats on PS–SiO_x/Si when thin films were exposed to DMF vapor. In fact, the transition to form giant mats on PS-SiO_x/Si involved an intermediate stage of forming multi-layered terraces at the early process of solvent annealing (Fig. 3A). At first we speculated that the formation of terraced droplets (i.e., multiple stacks of circular lamellae) through the undulation of the film thickness might have been due to the mismatch of the natural domain distance with the particular film thickness (commensurability) [12,13,37–42]. Upon exposure to solvent vapor, the film surface might have acquired an undulating thickness so that the film stature should have become quantized to form terraced droplets with height thickness of units of the nanodomain spacing [12,13,37–42]. However, the relief terraces reveal two unusual features. First, each layer within the terraces approximately has thickness 15–20 nm, only half of the inter-lamella spacing. Second, the terraced droplets are not at equilibrium. Long-term solvent annealing in DMF vapor brought about the formation giant mats via a transition from terraced droplets (Fig. 3A-c and A-d and B-a and B-b). This could not be explained by the incommensurability effect that eventually causes relief terraces at equilibrium [12,13]. Within the relief terraces at equilibrium, each lamellar layer is comprised of an entire PS-P4VP/P4VP-PS repeat unit (Fig. 3B-c) [12,13]. DMF is a good solvent for the P4VP block. Whereas in the presence of DMF vapor, the free surface was preferentially wetted by P4VP chains, the PS-grafted layer was favorably wetted by PS chains. If the lamellar layers had adopted the arrangement of alternately PS-P4VP/P4VP-PS layers, the PS chains within each lamellar layer should have been forced to unfavorably expose to the DMF vapor. Besides, each lamellar layer should have had the thickness of an entire repeat unit of lamella (Fig. 3B-c). Here we propose another packing mechanism for interpreting the metastability of P(S-*b*-4VP) terraces on PS-SiO_x/Si under DMF vapor. We speculate that within the DMF-annealed terraces on PS-SiO_x/Si, the layers pile up alternatively PS-P4VP layers from the substrate interface to the free surface (Fig. 3B-a). With the lamellar layers adopting such an arrangement, the P4VP chains were always exposed to DMF vapor but it inevitably imposed a high energy penalty at the contacts between the PS and P4VP chains. Therefore, these DMF-annealed terraces were still in metastable. Nevertheless, this lamellar packing was favorable for quick rearrangement of the terraced droplets to form the giant mats when long-term annealing was implemented. This arrangement of PS-P4VP layers also explains why every layer within the DMF-annealed terraces has half of the thickness of an entire PS-P4VP/P4VP-PS layer (Fig. 3B-b).

Results of TEM experiments shown in Fig. 4 confirm the hypothesis of the terraced stack of PS-P4VP layers on PS-SiO_x/Si for films exposed to DMF vapor. The cross-sectional TEM of the film with solvent annealing in DMF vapor for 30 min reveals terraced droplets (i.e., multiple stacks of PS-P4VP layers) (Fig. 4a). The top layers closest to the free surface display dark streaks consistent with P4VP domains, and the layers closest to the substrate interface show lighter streaks consistence with PS domains (see the inset). Long-time exposure in DMF vapor (360 min) caused the preferential formation of one single monolayer of PS-P4VP chains with the PS chains facing PS-SiO_x/Si and with the P4VP blocks facing outward to the air (Fig. 4b). As a result of the transition of the terraced droplets, the single monolayer spread over the scale of a few hundreds of nanometers on top of PS-SiO_x/Si.

3.2. *Hierarchical assembly of micelles on micro-patterned substrates in solvent vapors of varied selectivity*

Spin-coating micelles from 0.5 mass % led to a monolayer of spherical nanodomains covering over the surface of the patterned substrate. The thickness of the layer on the regions grafted by PS chains seems thicker than that on the PS-free areas (see Fig. S2). Consequently, globule-like, submicron structures are discerned for the films on the patterned substrate. The hierarchical assembly of

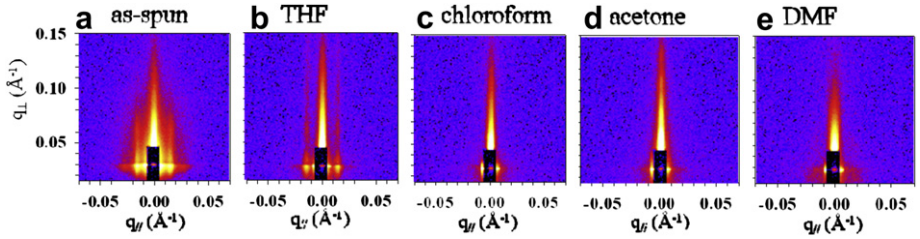

Fig. 2. 2D GISAXS patterns for thin films without (a) and with annealing in the solvent vapors: (b) THF, (c) chloroform, (d) acetone and (e) DMF. All the films were prepared by spin-coating from a 0.4 mass % polymer solution in the mixture of toluene and THF.

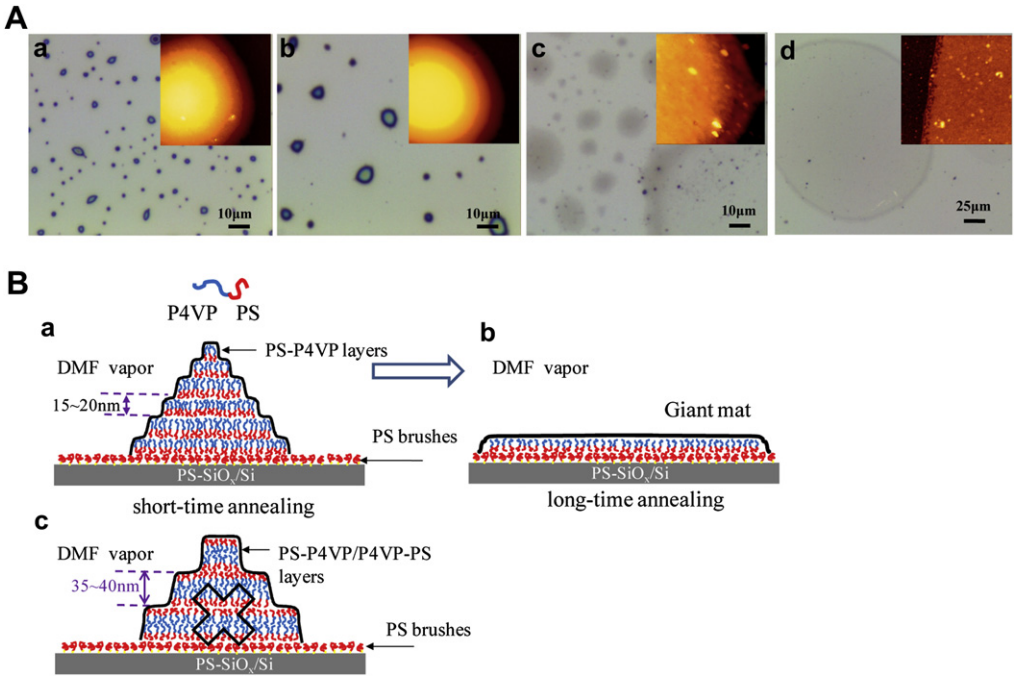

Fig. 3. (A) Reflection optical micrographs of P(S-*b*-4VP) films with an incomplete coverage on PS-SiO_x/Si after solvent annealing in DMF vapor for 10 (a), 30 (b), 90 (c) and 360 min (d). Insets show 2 × 2 μm^2 AFM topographies. (B) Schematic diagram of a symmetric P(S-*b*-4VP) terraced stack of PS-P4VP layers or PS–P4VP/P4VP–PS layers on PS–SiO_x/Si (a, left-handed side) and giant mat (b, right-handed side) in DMF vapor. The stack of PS–P4VP/P4VP–PS layers should be forbidden in DMF vapor since such a stack should have highly unfavorable contacts between PS chains and DMF vapor (c). Because DMF is a poor solvent for PS, the grafted PS chains should be more likely in a shrinkage conformation.

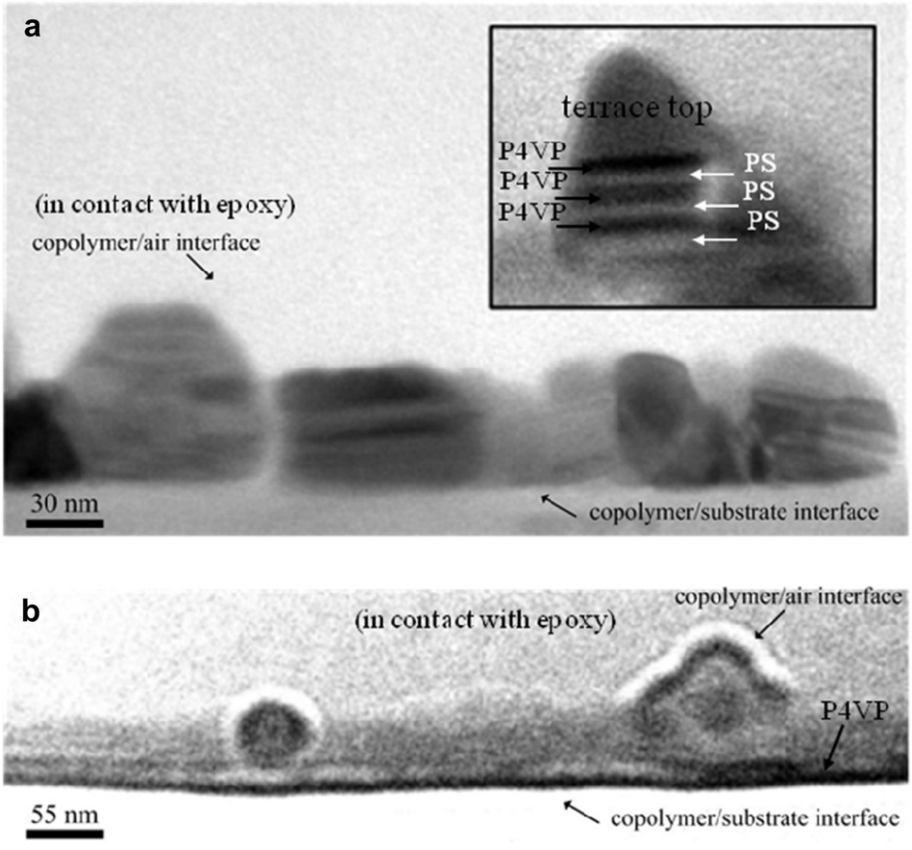

Fig. 4. Cross-sectional TEM images of P(S-*b*-4VP) samples annealed with DMF vapor for (a) 30 and (b) 360 min followed by solvent removal. Inset shows the high magnification of the cross-sectional TEM image of one terrace of multiple layers in the specimen (a), in which the dark regions of the terrace correspond to P4VP (preferentially stained with I_2) and the lighter regions correspond to PS. The flat regions correspond to the bottom of the terraced droplets whereas the contoured surface corresponds to the top of the terraced droplets. In the TEM images, the top regions are in contact with epoxy.

micellar films on a chemically patterned substrate could be achieved by exposing micelles to solvent vapors. Fig. 5 shows solvent-driven hierarchical ordering of the P(S-*b*-4VP) thin films on PS-grafted regions. After solvent annealing in the solvent vapors, the P(S-*b*-4VP) films reveal a high tendency to migrate onto the PS-grafted regions, leading to the formation of hexagonally packed micro-sized terraces or droplets. In contrast, the regions without grafting by PS chains reveal a featureless surface. The featureless surface originates either from the surface of SiO_x/Si under DMF vapor or from a wetting layer of P(S-*b*-4VP) monolayer thickness anchored with SiO_x/Si under THF, chloroform and acetone vapors.

Close scrutiny of the AFM images demonstrates that the droplets with exposure to THF vapor are comprised of spherical nanodomains and have a hemi-spherical cap. The hemispherical cap is analogous to the shape of common liquid droplets (Fig. 5a-3). The formation of droplets though dewetting was not completed and each of the droplets was connected with its nearest neighbors by two or three thread-shaped structures. In comparison, exposure to chloroform and acetone vapors led to the formation of terraced microstructures, each of which terraces comprised a stack of thin concentric lamellae. The lamellae within the terraced microstructures oriented parallel to the substrate surface. Such terraces that are comprised of parallel oriented circular disks have a tendency to adopt a flat top surface connected a curved side structure. This kind of facetted droplets has also been discerned for thermal-annealed P(S-*b*-MMA) thin films on SiO_x/Si by Croll et al. [8]. The growth rate of terraces under the two solvent vapors was very fast in comparison with the case of solvent annealing in THF vapor. Upon annealing in chloroform and acetone vapors for 1 or 2 h, the nanolamella-comprised terraces have completely formed, and the terraced shape has been at equilibrium (the data are not shown). In other words, further annealing for longer time intervals could not bring about other morphological changes at nanometer and micrometer scales.

In contrast, thin films with annealing in DMF vapor reveal different surface morphologies in self-assembled nanodomain and relief microstructure. The formation of relief microstructures with microscopically hexagonal order was also fast and completed at time intervals less than 30 min. Nevertheless, the shape of the relief microstructures was diverse, depending on microphase-separated nanodomains buried within the relief microstructures. Three types of relief microstructures, nanosphere-comprised, nanocylinder-comprised and nanolamella-comprised relief microstructures, were obtained for thin films with exposure in DMF vapor at different time intervals or with different solvent-annealing treatments (Figs. 5d and 6).

Among the three types of relief microstructures, the nanocylinder-comprised droplets frequently appear when the annealing time interval was less than 8 h in DMF vapor (Fig. 6a–d). After further exposure to DMF vapors for long time intervals, the relief microstructures could be repeatedly transformed between a nanocylinder-comprised and nanosphere-comprised terrace (Fig. 6e–g). Occasionally, the nanolamella-comprised terraces could be obtained (Fig. 6h & n). This result indicates that in DMF vapor, the three types of relief microstructures were not a thermodynamically stable microstructure. The shape of the relief microstructures was found to depend on their internal building blocks (i.e., microphase-separated nanodomains). The nanosphere-comprised relief microstructures have a terraced shape. The thickness of each layer within this type of terraces is thin, approximately 14–16 nm. In comparison, the nanocylinder-comprised droplets reveal a hemi-spherical cap, which is analogous to that of common isotropic liquids. However, the cap surface of the droplets was seamed with cylindrical wrinkles. Nevertheless, for the both types underneath appears a thin layer of P(S-*b*-4VP) of ca 12 nm being in close contact with the grafted PS.

For terraced microstructures with parallel-oriented nanolamellae, the thickness for each layer is ca 20 nm, which size is thinner than that for terraces forming in chloroform and acetone. Each layer thickness for the lamella-comprised terraces with exposure in DMF is nearly a half of the thickness of those lamellae with exposure in chloroform and acetone vapors. This result demonstrates that whereas the lamellae within the terraces in DMF vapor consist of a series of alternately PS-P4VP layers, the terraces in chloroform and acetone vapors are formed from the lamellar layers that piled up alternately PS-P4VP/P4VP-PS layers. Regardless of internal nanostructures, the relief microstructures have a microscopically hexagonal order, governed by the PS-grafted pattern (Fig. 6l–n).

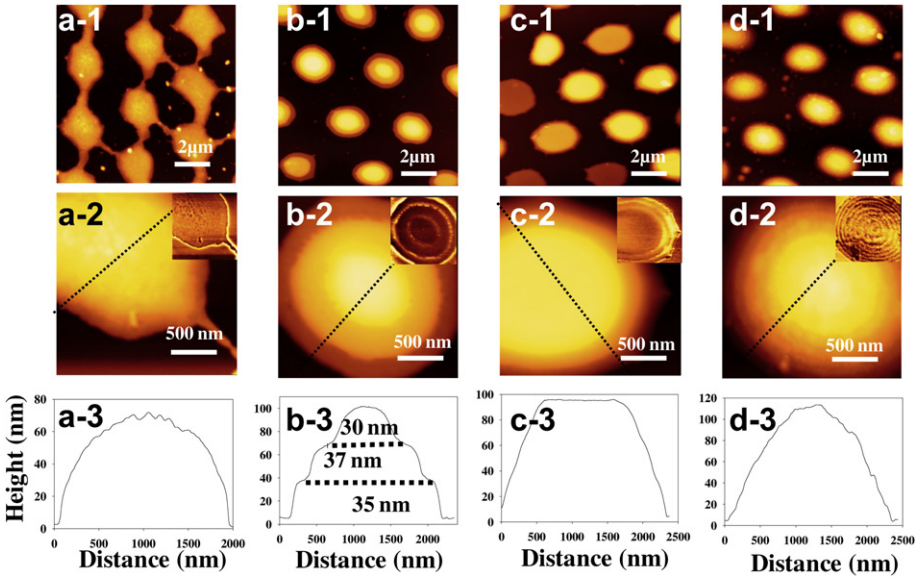

Fig. 5. 10 × 10 (top row, 1) and 2 × 2 μm^2 (middle row, 2) AFM topographic images, and height profiles (bottom row, 3) of thin films with 6 h exposure in vapors of (a) THF, (b) chloroform, (c) acetone, and (d) DMF on substrates with a PS-grafted pattern. The insets show phase images.

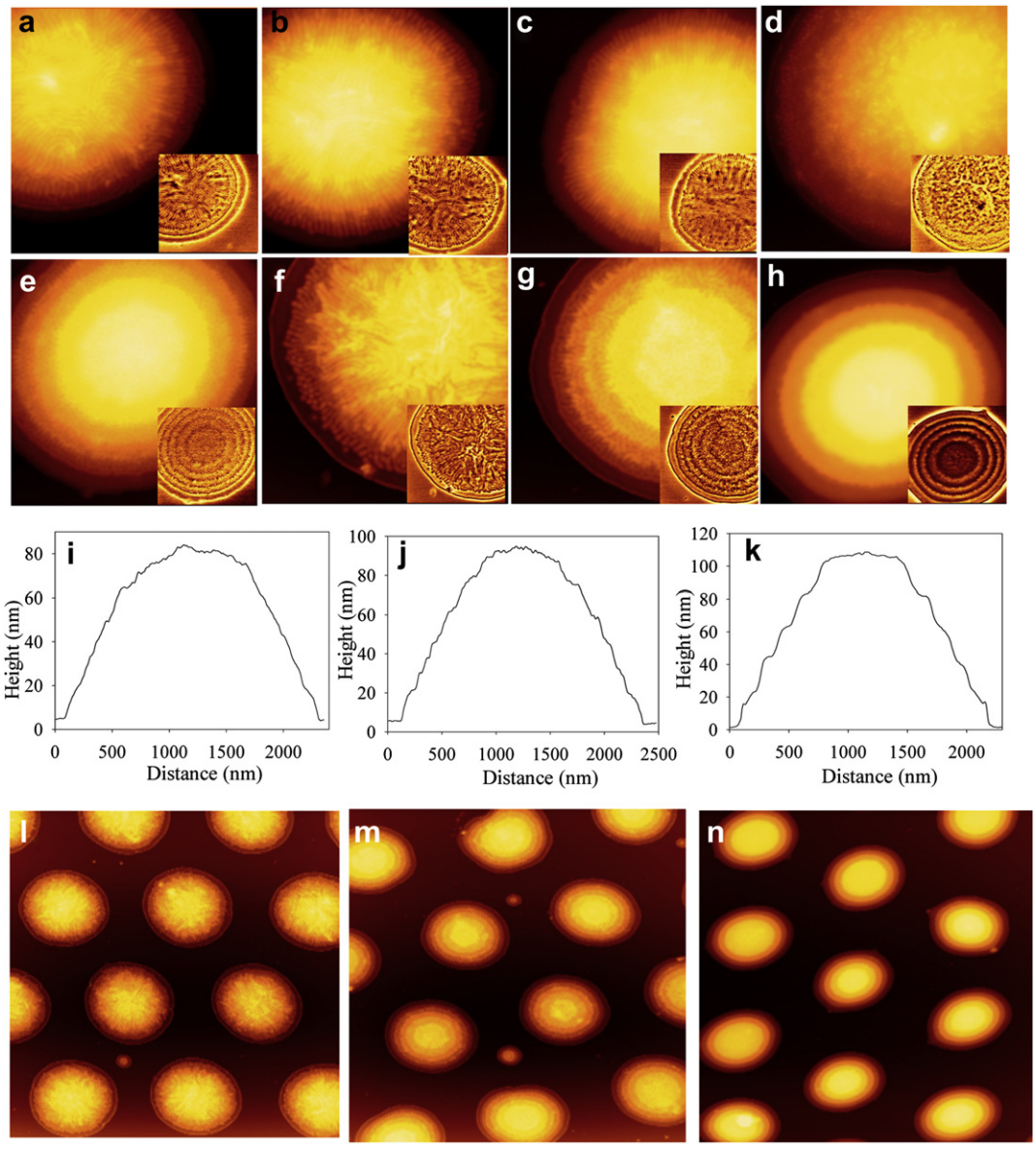

Fig. 6. $2 \times 2\ \mu m^2$ AFM topographic images of a thin film alternately with stepwise solvent annealing in DMF vapor and by AFM observations every 2 h of solvent annealing for (a) 2, (b) 4, (c) 6, (d) 8, (e) 10, (f) 12 and (g) 14 h, and with continuous exposure of 8 h (h). The insets show $2 \times 2\ \mu m^2$ phase images. The middle row (i–k) respectively shows the height profiles of images (c), (e) and (h). The bottom row (l–n) respectively shows $10 \times 10\ \mu m^2$ topographic images of solvent treatments (f), (g) and (h).

Here it is worth noting that no transformations from relief terraces to giant mats occurred on patterned substrates under DMF vapor. Instead, solvent annealing in DMF vapor caused various nanodomains (nanocylinders or nanospheres) that existed within the relief microstructures. Accordingly, we suggest the following scenario (Fig. 7). On the substrates with a PS-grafted pattern, if the terraces comprise a series of alternately PS-P4VP layers, DMF vapor makes the nanolamella-comprised terraces metastable because of unfavorable contacts between PS and P4VP chains at the inter-layer interface. Since DMF vapor imposes a high energy barrier for wetting of P(S-*b*-4VP) chains onto the PS-free surface, therefore the formation of giant mats via a microscopic transition from nanolamella-comprised terraces is not allowable on the patterned substrate. In order to reduce the unfavorable contacts between PS and P4VP chains, it is more favorable to form core–shell nanocylinders or nanospheres in which PS is the core and P4VP is the shell. With such a conformation, each PS core can be avoided to expose to DMF vapor because of isolation by the P4VP shell. This explains that the nanosphere-comprised or nanocylinder-comprised terraces are more favorable than the development of giant mats on the patterned substrate (see Fig. 7).

We have showed that the surface of initially as-spun thin films was dominated by spherical micelles. Solvent annealing in THF leads to the growth of cylindrical micelles via fusion of spherical micelles at the early stage and the development of sphere-dominated nanodomains through fission of cylindrical micelles at the late stage [48]. Here we consider that in DMF vapor, the repeated conversion of cylindrical and spherical micelles is due to the recycling process between fusion and fission. Mokarian-Tabari et al. have found cyclical flipping of morphology between parallel and perpendicular arrays of nanocylinders in P(S-*b*-EO) block copolymer thin films [11]. They attributed the orientational transition between perpendicular to parallel arrays to be related to solvent volume uptake since solvent annealing is a dynamic

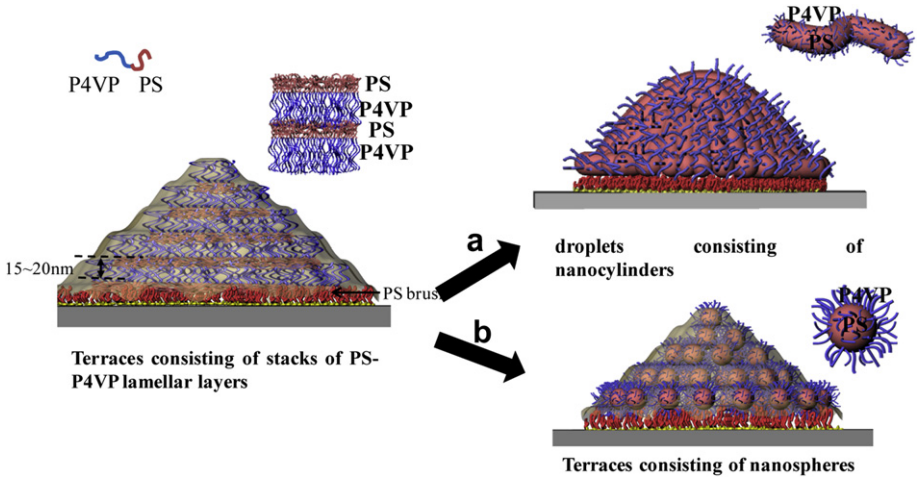

Fig. 7. Schematic diagrams of morphological variations from lamella-comprised terraces (a) to nanocylinder-comprised droplets or (b) to nanosphere-comprised terraces.

process. Such a dynamic process may account for the hierarchical self-assembly in response to phase transitions of P(S-*b*-4VP) films with exposure to DMF vapor. Whereas the relief microstructures consisted of either parallel nanolamellae or nanospheres reveal a terraced profile (Fig. 6e, g and h), the droplets with parallel-oriented cylinders reveal a hemi-spherical cap with wrinkling surface (Fig. 6a–d, f). In particular, the long axis of the parallel nanocylinders at the edge of the hemisphere cap oriented to the axial direction.

It has been found that when destabilized films have no lateral constraints in the plane on a flat substrate, a dewetting-induced stack of multiple layers of parallel nanocylinders commonly exhibits a terraced shape and also has random in-plane arrangement of parallel-orientation nanocylinders [49,50]. Without lateral constraints, the film surface can arbitrarily adjust itself by acquiring an undulating thickness so that the film stature becomes quantized to form terraced microstructures with height thickness of units of the nanodomain spacing. On the other hand, through dewetting to satisfy the film commensurability, internal defects can be prohibited and the ordering of buried nanodomains can become improved [44].

In contrast, within the circular geometry defined by the underlying PS-grafted layer, each droplet has a curved, circular base. Although in terms of the surface energy the spherical surface imposes less energy penalty than the terraced side surface, the droplets instead develop bends and tilts of nanocylinders, through which the long axis of nanocylinders is able to axially orient to the edge of the hemi-spherical cap. Our experimental observations show that the bends and tilts of nanocylinders are related to the balance of the elastic and the surface anisotropy of in-plane orientation of nanocylinders. Such a phenomenon has been observed in the system of droplets consisted of perpendicularly-oriented lamellae [7]. Since thin films with exposure to DMF vapors have an asymmetric wetting boundary on PS-SiO_x/Si, nanocylinders preferentially orient to the substrate surface. When the wetting boundaries of thin destabilized films are flat, there should be no lateral constrains on the in-plane orientation of parallel nanocylinders, and thus the arbitrary in-plane orientation could be allowable for nanocylinders. In the case of thin films having thickness gradient, the free surface is tilted by a given angle with respect to the bottom plate of SiO_x/Si. The curve surface causes coexistence of two states (see Fig. 8). The first state corresponds to the elastically undistorted state when the long-axis direction of nanocylinders has been parallel to the radial direction (as illustrated in Fig. 8a). Otherwise, nanocylinders have to be bent or tilted, making their long axis to be parallel to the radial direction of a microdroplet after distortion (as illustrated in Fig. 8b). On the other hand, it is likely that the bends and tilts of nanocylinders could lead to different extent of chain stretching or contraction at local areas, consequently yielding a hemispherical cap with irregular surface. We expect that internal defects may exist within the inner of the droplets due to the absence of film thickness quantumization [44].

Fig. 9 shows AFM images of microstructures and nanodomains within a thin film on PS-patterned substrates after stepwise exposure to solvent vapors of varied selectivity, in which each exposure in a solvent vapor took 6 h. As one can see, DMF vapor brought about the formation of either nanosphere-comprised or nanocylinder-comprised droplets whereas acetone and chloroform vapors led to terraces with lamellar nanodomains oriented parallel to the substrate surface. In THF vapor, the sphere-comprised

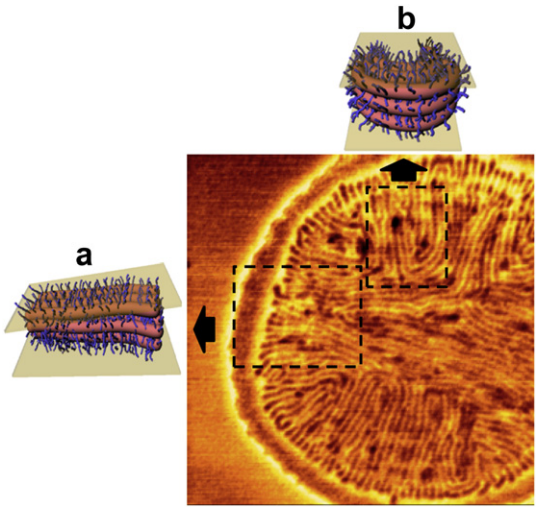

Fig. 8. Schematic illustration of cylindrical morphology according to the boundary tilting of block copolymer films of varying thickness. The long axis direction of nanocylinders *n* tends to be parallel to the radial direction of the circular microstructure to prevent splay deformation of the nanocylinders (a) whenever *n* deviates from the radial direction of the circular microstructure, the cylinders are bent (b). The AFM phase image corresponds to the surface morphology of one droplet consisted of nanocylinders with 6 h of exposure in DMF vapor.

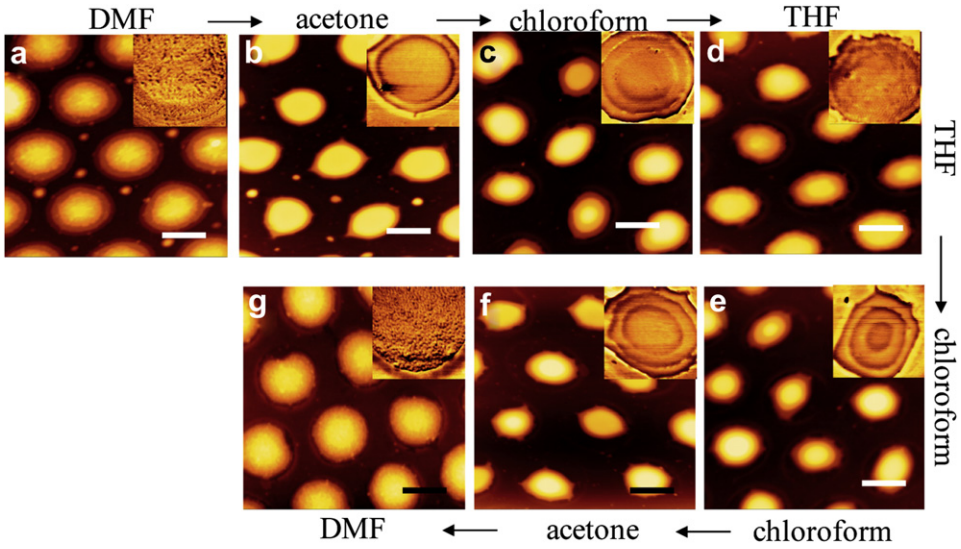

Fig. 9. AFM topographies of a thin film with 6 h-stepwise annealing in various solvent vapors in the sequence of DMF (a), acetone (b), chloroform (c), THF (d), chloroform (e), acetone (f) and DMF (g). Insets show 2 × 2 μm^2 the phase images of one relief microstructure (terrace or droplet).

droplets were obtained. As a result, switchable hierarchical structures could be obtained upon changing solvent vapor selectivity. We also notice that the relief microstructures with exposure to the PS-preferential solvent vapors have smaller diameter than those droplets with exposure to DMF vapor. The reduced diameter may be either migrating of certain P(S-*b*-4VP) chains from PS-grafted regions to PS-free regions to form a wetting layer or growing into high stature at expense of the diameter.

4. Conclusions

In summary, we demonstrate the responses of relief P(S-*b*-4VP) microstructures and internal nanodomains on a patterned substrate to different solvent vapors. As the P(S-*b*-4VP) microstructures comprise nanospheres or PS-P4VP-type lamellae with solvent annealing in DMF vapor or PS-P4VP/P4VP-PS-type lamellae with parallel orientation in acetone and chloroform vapors, the microstructure shape has a terraced profile. For exposure in DMF vapor, as the internal nanodomains transform from nanospheres or PS-P4VP layers to nanocylinders, the droplet shape switches from an isotropic layered morphology to a wrinkling spherical cap. In THF vapor, the microstructure shape has a hemispherical cap, which is analogous to that of common liquids. Furthermore, changing solvent selectivity leads to not only morphological transitions of microphase-separated nanodomains but also shape transformations of relief microstructures. These transitions and transformations are cooperatively in response to the stimuli imposed by solvent vapors of varied selectivity.

Acknowledgments

National Science Council provided supports (NSC-100-2628-E-008-007-MY3 and NSC-100-2120-M-008-001). The authors are grateful to Prof. Cheng-Yi Liu of National Central University, who kindly supplied the sapphire master mold for this study.

Appendix A. Supplementary data

Supplementary data related to this article can be found at http://dx.doi.org/10.1016/j.polymer.2012.10.031.

References

[1] Lehn JM. Science 2002;295:2400–3.
[2] Whitesides GM, Grzybowski B. Science 2002;295:2418–21.
[3] Stuart MAC, Huck WTS, Genzer J, Muller M, Ober C, Stamm M, et al. Nat Mater 2010;9:101–13.
[4] Kim TH, Hwang J, Hwang WS, Huh J, Kim HC, Kim SH, et al. Adv Mater 2008; 20:522–7.
[5] Kim TH, Huh J, Park C. Macromolecules 2010;43:5352–7.
[6] Kim BH, Shin DO, Jeong SJ, Koo CM, Jeon SC, Huang WJ, et al. Adv Mater 2008; 20:2303–7.
[7] Kim BH, Lee HM, Lee JH, Son SW, Jeong SJ, Lee S, et al. Adv Funct Mater 2009; 19:2584–91.
[8] Croll AB, Massa MV, Masten MW, Dalnoki-Veress K. Phys Rev Lett 2006;97: 204502-1–204502-4.
[9] Kim JU, Matsen MW. Soft Matter 2009;5:2889–95.
[10] Farrell RA, Kehagias N, Shaw MT, Reboud V, Zelsmann M, Holmes JD, et al. ACS Nano 2011;5:1073–85.
[11] Mokarrian-Tobari P, Collins TW, Holmes JD, Morris MA. ACS Nano 2011;5: 4617–23.
[12] Turner MS. Phys Rev Lett 1992;69:1788–91.
[13] Carvalho BL, Thomas EL. Phys Rev Lett 1994;73:3321–4.
[14] Qiao Y, Wang D, Buriak JM. Nano Lett 2007;7:464–9.
[15] Park S, Wang JY, Kim B, Russell TP. Nano Lett 2008;8:1667–72.
[16] Park S, Kim B, Wang JY, Russell TP. Adv Mater 2008;20:681–5.
[17] Aizawa M, Buriak JM. J Am Chem Soc 2005;127:8932–3.
[18] Aizawa M, Buriak JM. Chem Mater 2007;19:5090–101.
[19] Kim Y, Han H, Kim Y, Lee W, Alexe M, Baik S, et al. Nano Lett 2010;10:2141–6.
[20] Yun SH, Yoo SI, Jung JC, Zin WC, Sohn BH. Chem Mater 2006;18:5646–8.
[21] Boyen HG, Kästle G, Zürn K, Herzog T, Weigl F, Ziemann P, et al. Adv Funct Mater 2003;13:359–64.
[22] Spatz JP, Chan VZH, Möβmer S, Kamm FM, Plettl A, Ziemann P, et al. Adv Mater 2002;14:1827–32.
[23] Lohmueller T, Bock E, Spatz JP. Adv Mater 2008;20:2297–302.
[24] Chai J, Buriak JM. ACS Nano 2008;2:489–501.
[25] Peonemann KV, Abetz V, Simon PFW. Nat Mater 2007;6:992–6.
[26] Förster S, Antonietti M. Adv Mater 1998;10:195–217.
[27] Förster S, Plantenberg T. Angew Chem Int Ed 2002;41:688–714.
[28] Numes SP, Sougrat R, Hooghan B, Anjum DH, Behzad AR, Zhao L, et al. Macromolecules 2010;43:8079–85.
[29] Tseng WH, Chen CK, Chiang YW, Ho RM, Akasaka S, Hasegawa HJ. Am Chem Soc 2009;131:1356–7.
[30] Hsueh HY, Chen HY, She MS, Chen CK, Ho RM, Gwo S, et al. Nano Lett 2010;10: 4994–5000.
[31] Segalman RA, Yokoyama H, Kramer EJ. Adv Mater 2001;13:1152–5.
[32] Cheng JY, Ross CA, Thomas EL, Smith HI, Vancso GJ. Appl Phys Lett 2002;81: 3657–9.
[33] Kim SO, Solak HH, Stoykovich MP, Ferrier NJ, de Pablo JJ, Nealey PF. Nature 2003;424:411–4.
[34] Park S, Lee DH, Xu J, Kim B, Hong SW, Jeong U, et al. Science 2009;323: 1030–3.
[35] Park S, Kim B, Xu J, Hofmann T, Ocko BM, Russell TP. Macromolecules 2009; 42:1278–84.

[36] Park S, Wang JY, Kim B, Chen W, Russell TP. Macromolecules 2007;40:9059–63.
[37] Limary R, Green PF. Langmuir 1999;15:5617–22.
[38] Limary R, Green PF. Macromolecules 1999;32:8167–72.
[39] Masson JL, Limary R, Green PF. J Chem Phys 2001;114:10963–7.
[40] Coulon G, Russell TP, Deline VR, Green PF. Macromolecules 1989;22:2581–9.
[41] Anastasiadis SH, Russell TP, Satija SK, Majkrzak CF. Phys Rev Lett 1989;62:1852–5.
[42] Henkee CS, Thomas EL, Fetters LJ. J Mater Sci 1988;23:1685–94.
[43] Sun YS, Chien SW, Liou JY. Macromolecules 2010;43:7250–60.
[44] Sun YS, Chien SW, Wu PJ. Macromolecules 2010;43:5016–23.
[45] Sun YS, Chien SW, Liou JY, Su CH, Liao KF. Polymer 2011;52:1180–90.
[46] Lide DR. Handbook of chemistry and physics. 90th ed. Florida: CRC Press; 2009 [chapter 6].
[47] Chang CY, Lee YC, Wu PJ, Liou JY, Sun YS, Ko BT. Langmuir 2011;27:14545–53.
[48] Chang CY, Wu PJ, Sun YS. Soft Matter 2011;7:9140–7.
[49] Zoelen WV, Polushkin E, Brinke GT. Macromolecules 2008;41:8807–14.
[50] Zoelen WV, Asumaa T, Ruokolainen J, Ikkala O, Brinke GT. Macromolecules 2008;41:3199–208.